1-1-1994

Fatigue Strength of Electrogas Welds in Double-Hull Construction

Mark R. Kaczinski
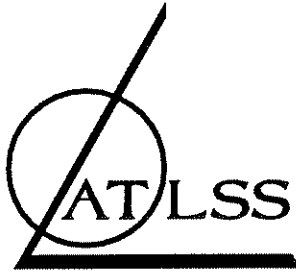
Eric J. Kaufmann

Follow this and additional works at: http://preserve.lehigh.edu/engr-civil-environmental-atlss-reports

Recommended Citation

Kaczinski, Mark R. and Kaufmann, Eric J., "Fatigue Strength of Electrogas Welds in Double-Hull Construction" (1994). ATLSS Reports. ATLSS report number 94-01:.
http://preserve.lehigh.edu/engr-civil-environmental-atlss-reports/196

ATLSS

Fatigue Strength of Electrogas Welds

In

Double-Hull Construction

by

Mark R. Kaczinski
Research Engineer

Eric J. Kaufmann
Research Engineer

ATLSS Report No. 94-01

January 1994

ABSTRACT

A new tanker design has been proposed which incorporates construction features that meet the needs for safe, economical and environmentally sensitive transport of oil products. This new tanker design, brand name Marc Guardian, incorporates 2.1 m × 2.4 m × 15.2 m (7'x8'x50') cellular modules consisting of both inner and outer hull plates which are curved to add strength and stability to the double-hull section. These cellular modules are then joined into 136-318 metric ton (150-350 ton) double-hull subassemblies which can be incorporated into new or converted tankers. The arched configuration on the hull plates is expected to reduce shipbuilding costs as much as 30 percent by reducing construction time with simplified joint details.

Current plans are for the 15.2 m (50 ft) tank modules to be fabricated in a vertical orientation. The two curved hull plates and cell web girder are joined with a single, continuous Electrogas weld (EGW) pass. The vertical EGW process was selected because it can achieve a high deposition weld rate (23 kg/hr or 43 lb/hr). Unfortunately however, the EGW, and related electroslag weld (ESW), have been previously identified as having poor fracture toughness in the weld metal and HAZ.

Because of the metallurgical uncertainties associated with the EGW process, the ATLSS Engineering Research Center at Lehigh University was contracted by Metro Machine Corporation to experimentally study the proposed EGW detail specified for use in the new Marc Guardian tanker. The primary objective of the experimental study was to determine the fatigue resistance of the longitudinal EGW used to join the hull plates and web girder of this unique double-hull vessel. A total of 20 full-scale, beam specimens which simulated the weld detail used in the tanker were fabricated and tested under constant amplitude, fully reversed, cyclic loads at the ATLSS Center's laboratory. The tests results were compared to existing fatigue resistance S/N curves for other longitudinally welded joints. In addition, a preliminary study of the weld metal fracture toughness and tensile properties was also conducted.

TABLE OF CONTENTS

1. INTRODUCTION

An experimental study was conducted of the fatigue resistance of longitudinal electrogas welds (EGW) used to join the web and top flange of beam specimens. The study was conducted at Lehigh University's ATLSS Engineering Research Center and the fatigue test specimens were fabricated by Metro Machine Corporation. The specimens simulate the weld detail used to join hull plates on a new double-hull tanker design. This new tanker design, the Marc Guardian, is illustrated in Figure 1. The tanker incorporates 2.1 m × 2.4 m × 15.2 m (7'x8'x50') cellular modules consisting of both inner and outer hull plates which are curved to add strength and stability to the double-hull section. The arched configuration is expected to reduce shipbuilding costs as much as 30 percent by simplifying construction details which then reduces the construction time and displaced weight of the vessel [1].

Current plans are for the 15.2 m (50 ft) modules to be fabricated in a vertical orientation. The two curved hull plates and cell web are joined with a single, continuous EGW pass. The vertical EGW process was selected because it can achieve a high deposition weld rate (23 kg/hr or 43 lb/hr). The EGW, and related electroslag weld (ESW), however have been previously identified as having poor fracture toughness in the weld metal and heat-affected-zone (HAZ). Several additional metallurgical characteristics of electrogas welds include the following [2].

1) The weldment resembles a casting with large columnar grains caused by the high heat input requirements, large weld pool, and slow cooling rate.
2) Grain boundary defects are common in the weld material which could possibly initiate fatigue crack propagation. In addition, corrosion, stress corrosion, and corrosion fatigue can occur more readily along these grain boundaries.
3) Improper weld conditions or techniques can result in significant inclusions, porosity and cracks.
4) The high heat input requirements create a large HAZ.

All of these characteristics, unfortunately, are known to be detrimental to the fracture toughness of welded joints. The well documented, premature fracture of the I-79 bridge over the Ohio River near Pittsburgh, PA in 1977 [3] and subsequent inspection reports from other ESW bridge sites [4] prompted the Federal Highway Administration (FHWA) to ban the use of electroslag welds in federally funded bridge projects. Because of the metallurgical uncertainty and failures associated with the EGW and ESW processes, the ATLSS Center was contracted by Metro Machine Corporation (U.S. Navy B.A.A. contract N00167-93-C-0004) to experimentally study the proposed EGW detail specified for use in the new Marc Guardian tanker.

The primary objective of the experimental study was to determine the fatigue resistance of longitudinal hull seam electrogas welds used in the construction of this unique double-hull vessel. A total of 20 specimens were tested under constant amplitude, fully reversed, cyclic loads at the ATLSS Center's laboratory. The tests were conducted on three different specimen configurations which included; 1) a longitudinal hull seam EGW detail alone; 2) a longitudinal

1

hull seam EGW intersected by transverse fillet welded attachments; and, 3) a longitudinal hull seam EGW intersected by butt welds made by the flux cored arc welding (FCAW) process.

The data were then compared to AASHTO [5] fatigue resistance S/N curves for other longitudinally welded joints (without transverse intersecting welds). Longitudinal welds are typically identified as a Type B or B' fatigue detail depending on the type of weld. For example, category B represents continuous longitudinal double fillet welds and full penetration groove welds with the backing bars removed. All other longitudinal welds are generally considered in category B'. Fatigue failures of the EGW were removed from specimens and examined to characterize the crack initiation sites. Finally, a preliminary study of the weld metal fracture toughness and tensile properties was also conducted.

2. FATIGUE TEST PROGRAM

2.1 Test Specimens

A fatigue test program was conducted on twenty full-scale specimens to study the fatigue resistance of longitudinal electrogas welds. All specimens were fabricated by Metro Machine Corporation in Norfolk, VA and contained full-length, longitudinal hull seam welds made by the electrogas welding process. This weld joins the web and top flange plates in a continuous single pass. As illustrated in Figure 2, three slightly different specimens were fabricated with common cross section dimensions and span lengths. The Type I specimens contained only the longitudinal hull seam EGW and no other attachment details. The Type IIA and Type IIB specimens were used to study the effect of intersecting the longitudinal EGW with either transverse butt welds or fillet welds. Two transverse butt welds, made by the FCAW process, in the web and top flange simulated spliced plate details and a fillet welded simulated bulkhead attachment were included near midspan in the Type IIA specimens. The Type IIB specimens contained only the two intersecting transverse butt weld details which had the weld reinforcement ground flush with the top surface of the top flange.

The cross section used for all three specimen types was designed to simulate the EGW detail required to join the two curved hull plates and web girder in the prototype double-hull structure. As illustrated in Figure 3, each of the two 25 mm (1 in.) thick plates used in the top flange of the specimen were placed at a 104 degree angle from the vertical axis of the 25 mm (1 in.) thick web. This 104 degree angle is equivalent to the angle of intersection of the curved hull plates with the web girder when the radius of curvature of the hull plate is equal to 5080 mm (200 in.). With the distance between web girders, and therefore the chord length, equal to 2.4 m (8 ft) the chord rise is 149 mm (5.85 in.). A 203 mm (8 in.) by 51 mm (2 in.) thick bottom flange was added to the web to create a 457 mm (18 in.) deep I-beam section which could be cyclically tested. The section properties of this asymmetric design were such that the longitudinal bending stress in the flared top flange was approximately two times higher than the stress in the bottom flange. The asymmetric design was used to ensure that under reversed cyclic loads fatigue failures would occur in the top flange joined by the EGW process. Actual cross section dimensions of several specimens were measured in the ATLSS laboratories and these measurements are tabulated in Table 1.

Each specimen was nominally 6.4 m (21 ft) in length with a constant bending moment in the 1.2 m (4 ft.) center span between load beam reaction points. Use of a full-scale specimen with a constant moment region enabled a large volume of the EGW detail to be subjected to a constant stress range.

Material properties, and thickness, of the top flange and web of the test specimens simulate what is specified for the prototype tanker design. A 25 mm (1 in.) thick, normalized, low carbon steel plate meeting American Bureau of Shipping (ABS) Grade AB/CS specifications was used for the top flange and a 25 mm (1 in.) thick, low carbon steel plate meeting ABS Grade AB/A

3

specifications was used for the web. Both materials have a specified minimum yield strength of 234 MPa (34 ksi).

The electrogas welded joint between the top flange and web was fabricated vertically in a 15.2 m (50 ft) high tower which was built exclusively for the Marc Guardian project. A mechanized, movable platform on the tower contains the necessary welding equipment and tracks the water-cooled copper shoe along the front face of the EGW. Within 100 minutes a 6.4 m (21 ft) single pass welded joint could be completed following all appropriate ASNI/AWS specifications [6,7] using an EG-82T-G self-shielding flux cored electrode.

Prior to conducting fatigue tests, the welds (EGW and FCAW butt welds) along the top flange of each beam specimen were thoroughly inspected visually and non-destructively using ultrasound equipment by Metro Machine Corporation. If any weld defects (i.e porosity, inclusions or cracks) above the acceptable size limits were detected in the EGW of the completed specimens, the specimen was rejected. The test program did not include fatigue tests of repaired electrogas welds.

2.2 Design of Experiments

All specimens were tested in four point bending in a single test station at Lehigh University's ATLSS Multidirectional Experimental Laboratory. The test station was designed to accommodate a pair of beams with a 6.1 m (20 ft) span length and a 1.2 m (4 ft) constant moment test section. Each beam was cyclically loaded with a single 489.3 kN (110 kip) digitally controlled, hydraulic actuator with an in-line 667.2 kN (150 kip) load cell. As illustrated in Figure 4, each actuator was centered on 1.2 m (4 ft) spreader beams which distributed the load equally to load points on the test specimen. The actuators were controlled by a personal computer to produce sinusoidal waveforms at frequencies from 1 to 3 Hz depending on the applied load range.

The first specimen to be tested, LB-2, was instrumented with six strain gages placed along the cross section at midspan to experimentally verify the beam's section properties by conducting a static load test. One of these strain gages was placed at the extreme fiber of the EGW and was used to calibrate the gages placed 51 mm (2 in.) from each edge of the top flange. Because of difficulties in placing strain gages on the irregular surface of the EGW, it was desirable to calibrate the applied cyclic load using gages placed on the top flange. The strain gage data, load cell measurements, and beam displacements recorded during the static load test were generally consistent with that predicted from strength of materials equations. Two additional specimens were also instrumented with three gages on the top flange to verify the ratio between extreme fiber stresses in the EGW and stresses in the top flange. In all three beams, the ratio of stresses in the flange 51 mm from the edge to stresses in the extreme fiber of the EGW was approximately equal to 1.03 as predicted by calculations. Therefore, on the remainder of the specimens only two strain gages were installed for calibration purposes.

Tests were performed in load control mode, although the stress range was determined using strain gages applied to the top flange as described above. The nominal stress range was periodically monitored using these strain gages to assure that the applied stress range remained constant. Displacements were also monitored and used to detect failure.

Each beam was typically inspected for cracks visually every 8 to 10 hours, however, this time interval was reduced for specimens being tested at the 276 MPa stress range. At first visual observation, the number of cycles, location, and surface length of the crack was recorded. Cycling was continued under load control until failure. As previously mentioned, failure was detected by monitoring the displacement of the specimens under a constant load range. A change in compliance of the beams that caused displacements to increase by 2.5 mm (0.1 in) was used to automatically shut off the test. By time this change in displacement had occurred, the crack usually extended across the full width of the top flange and approximately 100 mm (4 in.) down the web as shown in Figure 5.

A test matrix which indicates the number of beams tested at each of the three stress ranges, 138, 207 and 276 MPa (20, 30 and 40 ksi), is presented in Table 2. Although several Type I specimens were tested at each of the three stress ranges, the Type IIA and IIB specimens were only tested at 207 MPa (30 ksi). Since only four Type IIA and four Type IIB specimens were included in the project scope, testing was limited to the 207 MPa stress range to minimize the number of variables under consideration. The 138, 207 and 276 MPa stress range fatigue tests were conducted at 1, 1.75 and 3 Hz respectively with fully reversed load conditions. Under fully reversed load conditions the minimum and maximum stresses are equal and opposite in magnitude (i.e. +/- 69, 103 and 138 MPa).

3. MATERIAL TEST PROGRAM

To study the fracture toughness and tensile properties of the EGW and adjacent heat-affected-zone (HAZ) material, 54 charpy impact tests and three tensile tests were conducted. All material property test specimens were fabricated from sections cut from the end of specimen LB-10. Although these specimens were cut from beam specimen LB-10 after fatigue testing had been completed, subsequent material property tests should not be influenced by the presence of microcracks since the specimens were cut from near the end of the beam.

3.1 Tensile Tests

Three standard round tension test specimens with a 12.7 mm (0.5 in.) diameter cross section and 51 mm (2 in.) gage length were fabricated from the EGW material directly along the longitudinal axis of the weld. All tests were performed on a SATEC 2670 kN (600 kip) universal test machine in accordance with ASTM specification E8-91. Specimen extension was measured during the test with a 51 mm (2 in.) Linear Variable Differential Transformer extensometer and pre- and post-test reduction in area and elongation measurements were made with a digital caliper.

3.2 Charpy Impact Tests

Fifty-four Charpy V-notch impact toughness test specimens were fabricated in several orientations from the electrogas weld, HAZ, and base metal materials as shown in Figure 6. Two sets, each consisting of 18 specimens were fabricated from the weld material in the T-L orientation (i.e. stresses transverse to the weld and notch direction along the weld). In one set, the notch was placed in the direction of welding (specimen T-L(T)); and in the other, the notch was placed opposite the direction of welding (specimen T-L(B)). An additional set of 18 specimens were fabricated from the weld material in the L-T orientation. Eighteen HAZ material charpy specimens were made in the T-L orientation with the notch centered as close to the weld fusion line as possible. A set of 12 base metal specimens were also fabricated and tested. Each set was tested at temperatures ranging from -60 to +70 degrees C (-76 to +158 degrees F) following ASTM specification E-23.

4. TEST RESULTS

4.1 Fatigue Tests

A summary of fatigue test results for the Type I, Type IIA and Type IIB specimens are presented in Tables 3-5. Each table indicates the applied stress range, number of cycles to failure, and location of fatigue crack initiation. This information is also presented in a series of S/N data plots which include the AASHTO fatigue curves for categories A through C. The AASHTO curves correspond to the lower 95 percent confidence limit (97.5 percent survival limit) of a large database of conventionally welded joint details. As discussed previously, category B and B' are the applicable fatigue resistance curves for longitudinally welded joints.

Figure 7 is a plot of all fatigue failures found in the longitudinal hull seam EGW which did not initiate at either the transverse fillet or transverse butt welds. Data from all 12 Type I specimens, as well as Type IIB specimens LB-7(2) and LB-8(2) (which happen to also fail due to cracking in the EGW) are included in the plot and considered for the statistical analysis. The only data excluded from the statistical analysis are those specimens which did not fail in the EGW and are plotted as runouts. Runouts may belong to a population which is represented by the constant amplitude fatigue limit (CAFL). The CAFL is indicated by the horizontal line in the S-N plot and is not determined by a regression analysis. If the runouts were included in the regression analysis to determine the S-N plot, an increase in variance would be obtained. This increase in variance would, paradoxically, cause a decrease in the lower confidence limit.

The mean line of the data, assuming a slope of 3.0, is shown with a short dotted line which lies above the category B fatigue curve. The 97.5 percent survival limit is also plotted as a dashed line. This lower limit falls slightly above the category B' fatigue curve which shows that the data are consistent with the database for ordinary longitudinal welds. The B' S-N curve can therefore be used for the design of these EGW details. It should be noted that all failures, even those caused by extreme porosity or cold cracks, were above the category B' fatigue curve. Upon further examination, if failures from these large weld defects were eliminated from the data set all points would be above the category B curve. These results are consistent with the recent findings of Fisher, et.al [8] which also concluded that category B' is a safe lower bound fatigue design curve for degraded longitudinal welds which may include porosity, solid inclusions and cold cracks.

Figure 8 is a plot of fatigue failures in the Type IIA specimens. The transverse butt welds and transverse web attachments on these specimens are classified as category C fatigue details. Had the weld reinforcement been ground flush on the transverse butt welds, this detail could have been classified as category B. As expected, these details had a lower fatigue strength than the longitudinal EGW and all fatigue cracks were identified as initiating at either the toe of the fillet weld joining the simulated bulkhead attachment or the transverse butt weld. A photograph of a typical failure at the toe of the weld reinforcement is shown in Figure 10. Although no failures were obtained in the EGW, it can be assumed that the fatigue life of the longitudinal EGW is at least as long, if not longer, than the transverse weld details.

7

A plot of fatigue failures in the Type IIB specimens is presented in Figure 9. Two of the four specimens (LB-7(2) & 8(2)) failed in the EGW and were presented in Figure 7. These two data are presented as runouts in Figure 9 since the Type IIB weld detail did not fail. One of the two specimens failed at the toe of the unground transverse butt weld. The second Type IIB detail failed at the intersection of the EGW and transverse butt weld. A post test examination of the crack surface revealed that a significant amount of wormhole porosity occurred at this location. A photograph of this defect is presented in Figure 11 and it is encouraging to note that a discontinuity of this magnitude in the EGW does not dramatically effect the fatigue strength of this detail.

4.2 Characterization of Fatigue Crack Initiation Sites

The fracture surfaces of several fatigue specimens were examined visually to identify the location or locations where fatigue cracks initiated. The examination focused on those fractures which appeared to initiate in the EG weld region. Several of the crack surfaces were examined in greater detail with the scanning electron microscope (SEM) in cases where the initiating defect was too small to be observed visually or the origin of the defect was not clear.

Figures 11-14 show views of several fractures which initiated in the EG weld region which are representative of the types of initiating defects which were observed. The largest and most pronounced crack initiating defects observed were weld porosity as shown in Figure 11. Fatigue cracks are seen to initiate from several of these pores and propagate internally as penny shaped cracks until coalescing into a single crack.

The majority of fatigue cracks were observed to initiate at the weld toe of the EG weld along the top flange surface (see Figure 12). These cracks were found to initiate from several types of weld toe microdiscontinuities such as overlaps and hot cracks (see Figure 15). In one case hot cracking was identified by x-ray surface analysis as originating from copper solution in the weld metal undoubtedly introduced by arcing on or melting of the copper cooling shoes due to poor shoe cooling.

Figure 13 illustrates fatigue cracking in two test specimens which were attributable to weld surface irregularities. The ripple in the weld surface found in both EG and ES welds did not appear to be a significant factor in initiating these failures although the crack origin in one test specimen coincided with the edge of a surface ripple. The initiation site was found in both specimens to be small slag inclusions approximately 1 mm in depth at the weld surface. Figure 16 is an SEM micrograph of the crack surface of Type I Specimen 3-1. This micrograph illustrates the slag inclusion surface defect which initiated cracking.

Fatigue cracking in two test specimens was observed to initiate at the interior flange surface at the web-flange fillet as seen in Figure 14. These were clearly cracks which developed during fabrication since the surfaces were covered with a layer of corrosion product from exposure to the atmosphere. The crack in Type IIB specimen LB-7 was approximately 4 mm (0.157 in.) deep and 8 mm (0.315 in.) wide while the crack in Type I specimen LB-1 was 8 mm

8

(0.315 in.) deep and 11 mm (0.433 in.) wide. SEM examination showed they were intergranular (IG) cracks as seen in Figure 17. The grains appear elongated in the micrographs due to the columnar microstructure of the weld metal. IG cracking is usually associated with hydrogen induced cracking in welds. Grinding marks on the surface of the weld indicated there may have been an irregularity during welding which occurred at these locations. Fatigue strengths of these two beams with intergranular cracking still exceeded the Category B' S-N curve.

4.3 Material Property Tests

Results of the three all weld metal tensile tests are listed in Table 6 and a plot of the stress-strain curve for these three specimens is shown in Figure 18. By examining the results in Table 6 it can be seen that the measured tensile strength of all three specimens meet or exceeds the minimum AWS specified tensile strength requirements of 551 MPa (80 ksi) for EG8XT-X electrodes. As can be seen in Figure 18, the recorded stress-strain response of specimen A-1 was different than the other specimens. A visual examination of the test specimen fracture suggested that the failure occurred at a flaw in the specimen. A more thorough study under the Scanning Electron Microscope (SEM) revealed that the flaw was a 2-3 mm (0.1 in.) diameter void in the weld metal. Weld defects such as porosity and slag inclusions generally have little effect on weld metal yield strength but have a significant effect on ductility in the tension test as the test data show.

Charpy impact test results are plotted in Figures 19 and 20 and tabulated in Table 7. Figure 19 shows a comparison of the base metal, weld metal, and HAZ notch toughness. Although ABS Grade CS base plate does not have CVN impact test requirements, the base metal test results show that the 25 mm (1 in.) thick material readily satisfies the CVN requirements of all other ordinary strength ABS Grades which have impact toughness requirements including the most severe requirement of 19J at -40°C (14 ft-lbs at -40°F) (T-L) for Grade E.

The weld metal CVN results indicate a reasonable level of notch toughness which satisfies the AWS requirement of 27J at -29°C (20 ft-lbs at -20°F) for EG82T-X electrodes. As is also observed in electroslag weld metal, the measured notch toughness of the electrogas weld metal is slightly lower in specimens notched in the direction of welding. These data form the lower bound of the weld metal test data seen in Figure 19. This has been attributed to the columnar solidification structure of the weld metal in the ESW process and is likely the case for the EGW process as well.

As is expected in a high heat input process such as EGW, a significant reduction in notch toughness in the grain coarsened region of the HAZ was observed. The test data show an upward shift in the base metal transition temperature of at least 60°C, however, the resulting notch toughness is still comparable to that of the weld metal.

Figure 20 shows the weld metal test data including the results obtained from specimens notched transverse to the welding direction. These resulted in the lowest absorbed energies for all orientations tested. Since this represents an orientation of significance in applications where

9

applied loads are longitudinal, such as in double-hull ships, further characterization of the fracture properties of EG welds and their directionality would be desirable.

5. SUMMARY AND CONCLUSIONS

From the results of this study to determine the fatigue resistance of longitudinal hull seam electrogas welded details, the following conclusions and recommendations can be made.

1. A conservative lower bound estimate for the fatigue strength of longitudinal electrogas welds is the AASHTO category B' S/N curve. All fatigue failures, including those caused by significant weld metal porosity or cold cracks, were above the category B' curve.

2. The limited data on Type IIA and Type IIB details are consistent with AASHTO category C fatigue strengths.

3. A pilot study on the mechanical properties of the EGW material indicates that an acceptable level of notch toughness and ductility is present to minimize the possibility of weld metal fracture.

4. Several of the EGW failures resulted from large porosity defects which were undetected by the non-destructive inspection techniques. These findings indicate that existing ultrasonic testing procedures/transducers used to inspect the geometrically complex specimens are not reliable. The ultrasonic inspection method used an accept/reject response standard similar to ABS inspection criteria for conventional ship hull welds. Therefore, improvement in the ultrasonic interpretation of acceptable porosity limits is needed for electrogas welds.

5. Additional research should focus on developing and testing reliable, yet practical, EGW repair procedures.

6. REFERENCES

1.   The Philadelphia Inquirer, June 28, 1992, pp. C8-C9.

2.   Raman, A.
      ELECTROSLAG WELDS: PROBLEMS AND CURES,
      Welding Journal, American Welding Society, December 1981, pp.17-22.

3.   Fisher, J.W., Pense, A.W., and Housammann, H.
      ANALYSIS OF CRACKING OF I-79 BRIDGE AT NEVILLE ISLAND, Proceedings from
      the Fracture Problems in the Transportation Industry Fall Convention, Detroit, MI, October,
      1985.

4.   Pense, A.W., Wood, J.D., and Fisher, J.W.
      RECENT EXPERIENCES WITH ELECTROSLAG WELDED BRIDGES, Welding
      Journal, American Welding Society, December, 1981, pp. 33-42.

5.   American Association of State Highway and Transportation Officials
      STANDARD SPECIFICATIONS FOR HIGHWAY BRIDGES, 15TH Edition, Washington,
      D.C., 1992

6.   American Welding Society
      RECOMMENDED PRACTICES FOR ELECTROGAS WELDING, ASNI/AWS C 5.7-89

7.   American Welding Society
      SPECIFICATION FOR CARBON AND LOW-ALLOY STEEL ELECTRODES FOR
      ELECTROGAS WELDING, ASNI/AWS A 5.26-91

8.   Fisher, J.W., et. al.
      STRUCTURAL FAILURE MODES FOR ADVANCED DOUBLE HULL FATIGUE AND
      FRACTURE FAILURE MODES, Final Report for Cooperative Agreement N00014-91-CA-
      0001, TDL 91-01 Phase 1.3A, Lehigh University, Bethlehem, PA, March 1993

7. ACKNOWLEDGEMENT

8. TABLES

Dimension	Actual Measurements (mm)	Dimension	Actual Measurements (mm)
D	451 - 459	TW	25.7 - 26.4
DEGW	433 - 438	WTF	200 - 210
TTF	25.9 - 26.4	WBF	202 - 206
TBF	50.8 - 51.8	-	-

Note: 1 inch = 25.4 mm

Table 1 - Measured Cross Section Dimensions of Specimen

Stress Range (MPa)	Type I Specimens	Type IIA Specimens	Type IIB Specimens
138	4	-	-
207	5	4	4
276	3	-	-

Note: 1 ksi = 6.89 MPa

Table 2 - Test Matrix

Specimen	Sr (MPa)	Cycles to Failure	Failure Location
LB-1	138	3,987,900	Bottom Flange
LB-2	276	126,300	EGW
LB-3	276	298,600	EGW
LB-4	207	799,800	EGW
LB-5	138	7,000,000	Bottom Flange
LB-6	207	520,200	EGW
LB-7	207	1,523,200	Bottom Flange
LB-8	138	3,107,300	Bottom Flange
LB-9	138	5,357,300	Bottom Flange
LB-10	207	983,800	EGW
LB-11	207	1,504,600	Bottom Flange
LB-12	276	245,000	EGW (1)

Notes :

1 - Failure outside test region where Sr=241 MPa.

Table 3 - Data for Type I Specimens

16

Specimen	Sr (MPa)	Cycles to Failure	Failure Location (1)
LB-1(2)	207	211,900	Bulkhead
LB-2(2)	207	646,000	Transverse Butt and Bulkhead
LB-3(2)	207	489,300	Bulkhead
LB-4(2)	207	466,600	Transverse Butt

Notes:

1 - All failures initiated at the weld toe.

Table 4 - Data for Type IIA Specimens (with Bulkhead Attachments)

Specimen	Sr (MPa)	Cycles to Failure	Failure Location
LB-5(2)	207	487,900	Transverse Butt(1)
LB-6(2)	207	206,000	EGW(2)
LB-7(2)	207	753,800	EGW(3)
LB-8(2)	207	656,500	EGW

Notes:

1 - Failure initiated at the weld toe.
2 - Failure at intersection of EGW and Transverse Butt weld.
3 - Failure outside test region where Sr=181 MPa.

Table 5 - Data for Type IIB Specimens (without Bulkhead Attachment)

Specimen	Yield Strength (MPa)	Tensile Strength (MPa)	Elongation	Reduction in Area
A-1	448	600	17.2%	28.8%
A-2	421	579	27.4%	57.1%
A-3	414	565	29.7%	65.5%

Note: 1 ksi = 6.89 MPa

Table 6 - Results of Tensile Tests on EGW Metal

Specimen	Temperature (Celsius)	Energy (J)	Specimen	Temperature (Celsius)	Energy (J)
A - 1	21.5	111	B - 1	21.5	76
A - 2	21.5	96	B - 2	21.5	-
A - 3	21.5	79	B - 3	21.5	77
A - 4	21.0	88	B - 4	21.5	89
A - 5	0	56	B - 5	0	68
A - 6	0	47	B - 6	0	66
A - 7	0	56	B - 7	0	68
A - 8	-20	37	B - 8	-20	30
A - 9	-20	31	B - 9	-20	27
A - 10	50	157	B - 10	50	133
A - 11	50	161	B - 11	50	115
A - 12	-40	22	B - 12	-40	11
A - 13	-40	30	B - 13	-40	20
A - 14	-60	12	B - 14	-60	12
A - 15	-60	12	B - 15	-60	11
A - 16	70	163	B - 16	70	147
A - 17	70	153	B - 17	70	152
A - 18	70	153	B - 18	70	134

Notes:

    1 - Specimen A from weld metal in T-L(T) orientation
    2 - Specimen B from weld metal in T-L(B) orientation
    3 - 1 Ft-Lb = 1.356 J and $T_F = 1.8 \times T_C - 32$

Table 7 - Charpy V-Notch Data

Specimen	Temperature (Celsius)	Energy (J)	Specimen	Temperature (Celsius)	Energy (J)
C - 1	21.5	57	D - 1	21	57
C - 2	21.5	69	D - 2	21	41
C - 3	21.5	64	D - 3	21	65
C - 4	0	47	D - 4	-20	19
C - 5	0	47	D - 5	-20	27
C - 6	0	57	D - 6	-60	9
C - 7	-20	41	D - 7	-60	11
C - 8	-20	27	D - 8	-40	16
C - 9	-20	20	D - 9	-40	12
C - 10	50	88	D - 10	0	14
C - 11	50	92	D - 11	0	16
C - 12	-40	20	D - 12	0	42
C - 13	-40	24	D - 13	45	62
C - 14	-60	14	D - 14	45	54
C - 15	-60	11	D - 15	45	69
C - 16	70	111	D - 16	65	85
C - 17	70	117	D - 17	65	88
C - 18	70	94	D - 18	65	99

Notes:

    1 - Specimen C from weld metal in L-T orientation
    2 - Specimen D from HAZ material in T-L orientation
    3 - 1 Ft-Lb = 1.356 J and $T_F = 1.8 \times T_C - 32$

Table 7 - Charpy V-Notch Data (Cont.)

Specimen	Temperature (Celsius)	Energy (J)
E - 1	21	153
E - 2	21	144
E - 3	21	146
E - 4	-20	89
E - 5	-20	92
E - 6	-60	30
E - 7	-40	54
E - 8	-40	68
E - 9	0	125
E - 10	0	111
E - 11	50	155
E - 12	50	133

Notes:

1 - Specimen E from base metal in T-L orientation
2 - 1 Ft-Lb = 1.356 J and $T_F = 1.8 \times T_C - 32$

Table 7 - Charpy V-Notch Data (Cont.)

9. FIGURES
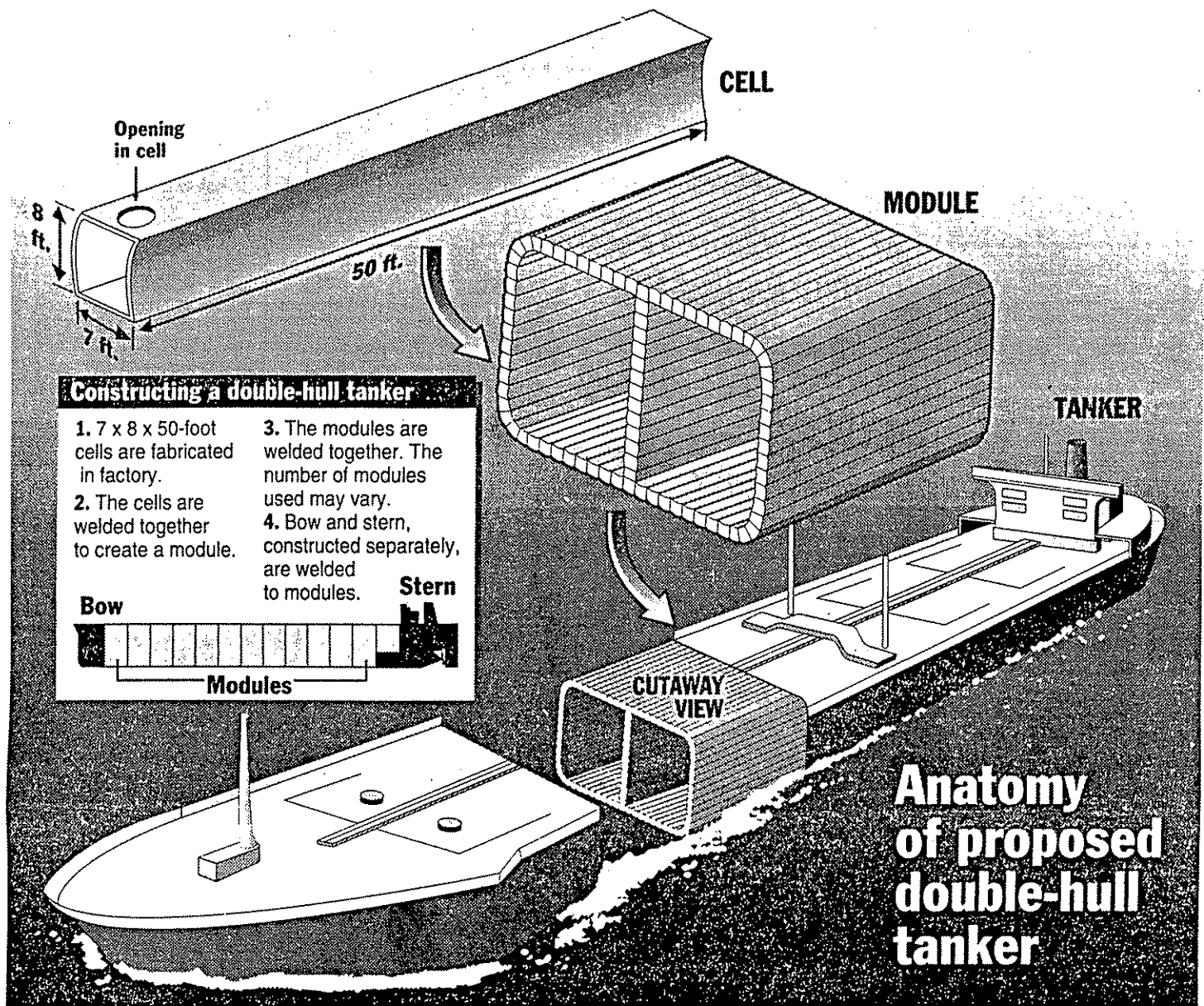
CELL

Opening in cell

8 ft.

7 ft.

50 ft.

MODULE

TANKER

Constructing a double-hull tanker

1. 7 x 8 x 50-foot cells are fabricated in factory.

2. The cells are welded together to create a module.

3. The modules are welded together. The number of modules used may vary.

4. Bow and stern, constructed separately, are welded to modules.

Bow ... **Stern**

Modules

CUTAWAY VIEW

Anatomy of proposed double-hull tanker

Figure 1 - Schematic of the Marc Guardian Tanker

Type I Specimen

- 6400 mm (21")
- 152 mm (6") typ
- P ⟷ 1219 mm ⟷ P (14")
- 457 mm (18")

Type II A Specimen

- ℄ Simulated Bulkhead Attachment
- 3200 mm (10'-0")
- 3200 mm (10'-0")
- 457 mm (18")
- 2667 mm (8'-9")
- 762 mm (2'-6")
- 2667 mm (8'-9")
- Full Penetration Butt Weld Detail (Web & Top Flange Only)

Type II B Specimen

- 6400 mm (21')
- 2667 mm (8'-9")
- 762 mm (2'-6")
- 2667 mm (8'-9")
- Full Penetration Butt Weld Detail (Web & Top Flange Only)
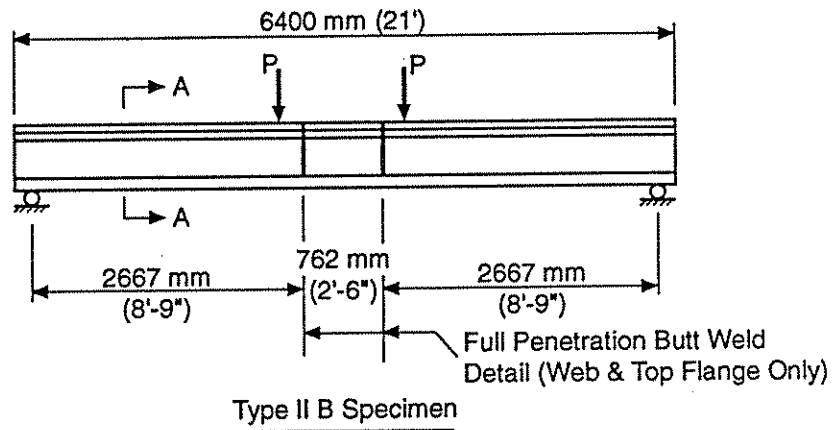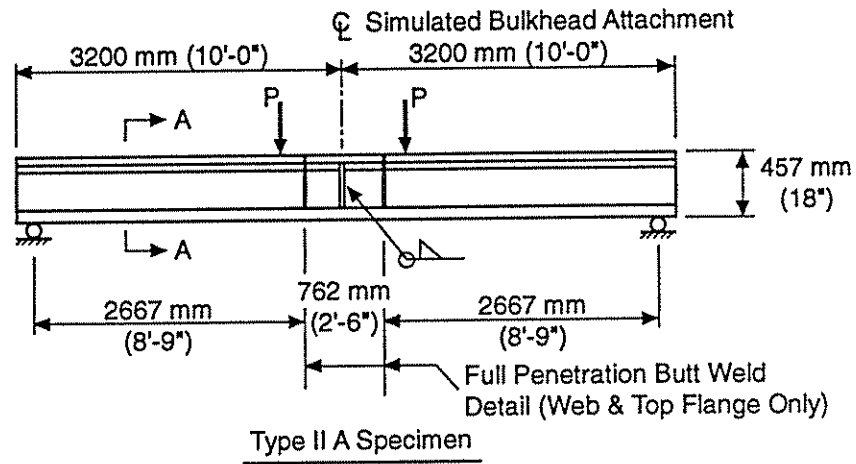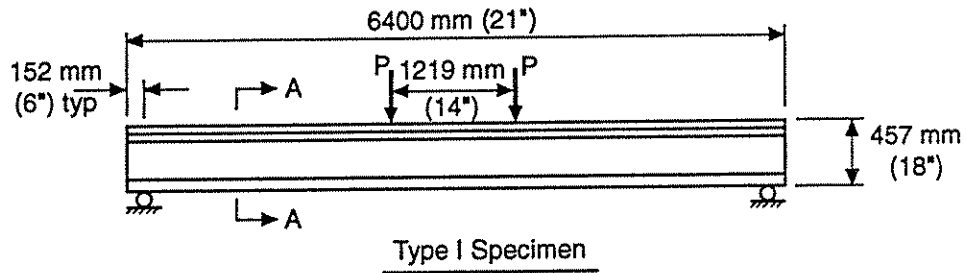
Figure 2 - Type I, Type IIA and Type IIB Specimen Details
(Section A-A illustrated in Figure 3)

203 mm
(8")

Electrogas Weld

25 mm
(1")

25 mm
(1")

356 mm
(14")

457 mm
(18")

51 mm (2")

203 mm
(8")
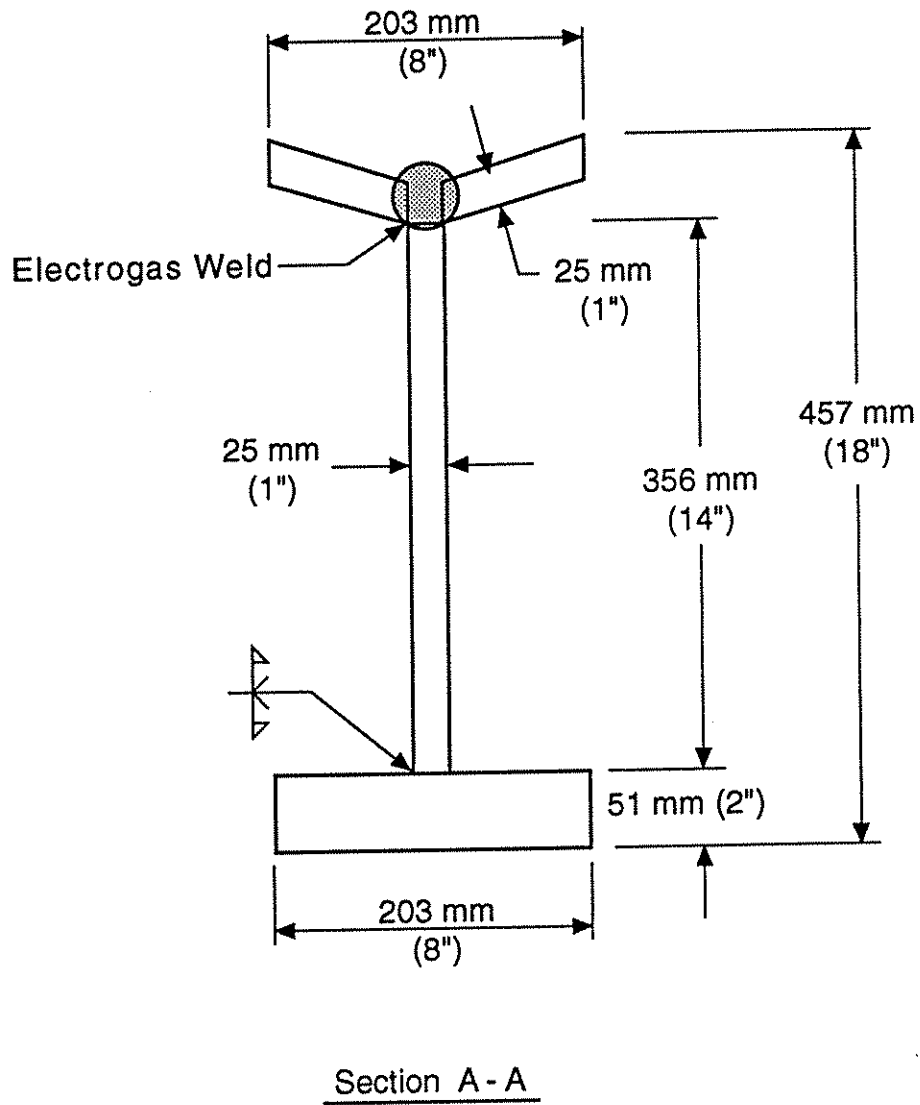
Section A - A

Figure 3 - Test Specimen Cross Section

25
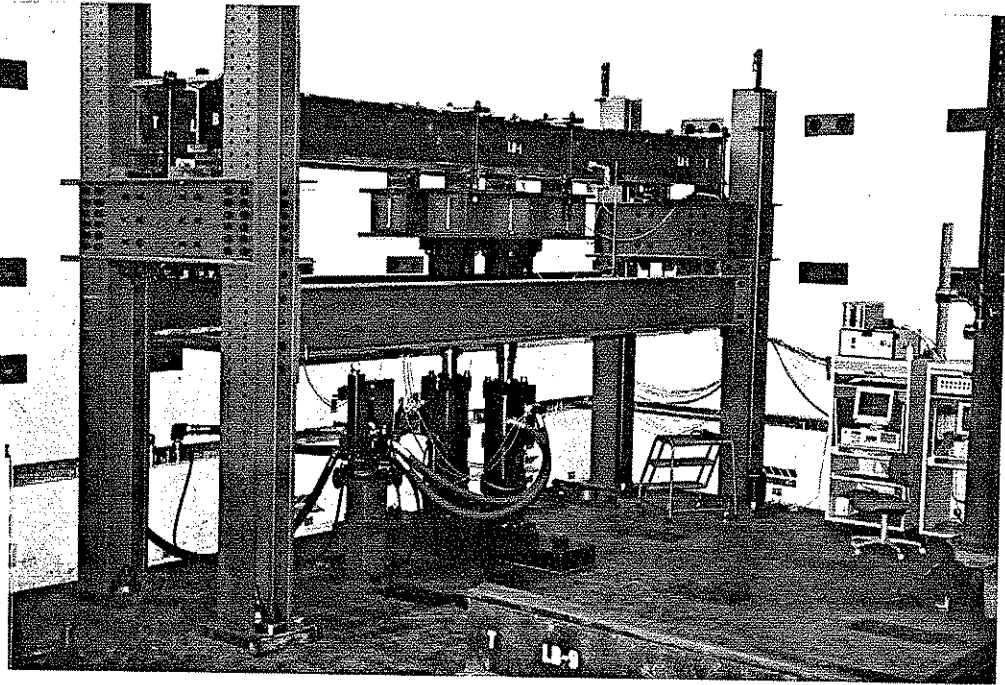
Figure 4 - Test Setup in ATLSS Laboratory (4/93/50-4)
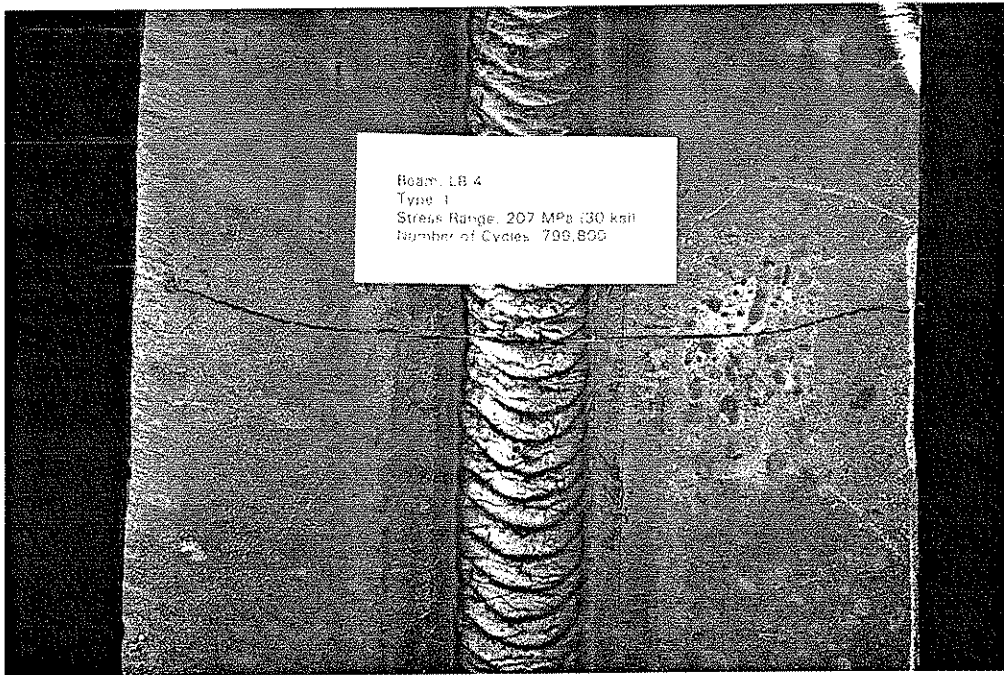
a) Crack Across Top Flange of Specimen (9/93/2-11)

Beam: LB-4
Type: I
Stress Range: 207 MPa (30 ksi)
Number of Cycles: 799,800
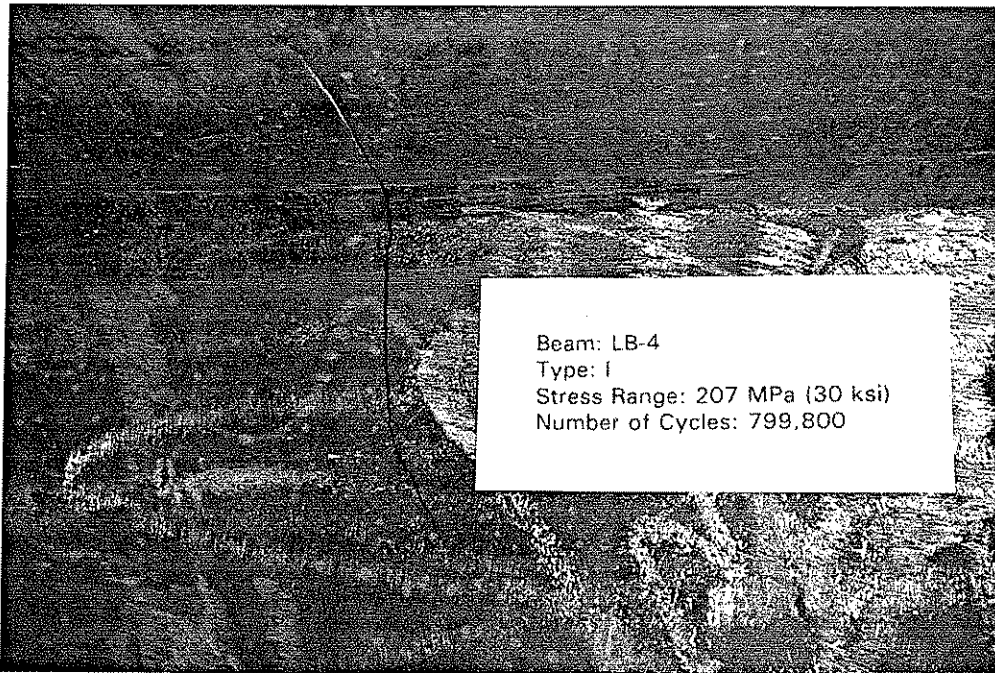
b) Crack Through Web of Specimen (9/93/3-2)

Figure 5 - Failure in Type I Specimen LB-4 at 799,800 cycles
(Crack size typical of all specimens)

Weld Direction
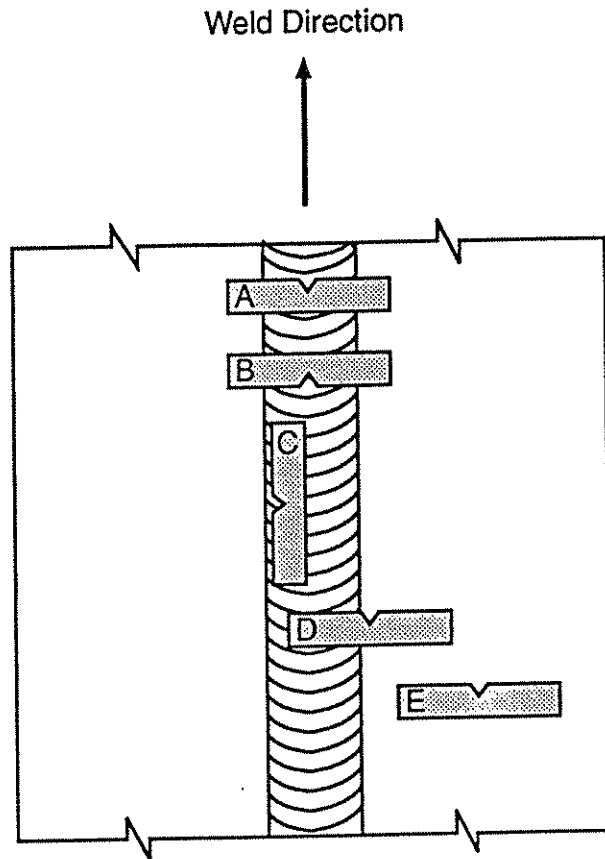
Specimen	Location		Number Tested
A	Weld Metal	T-L (T)	18
B	Weld metal	T-L (B)	18
C	Weld Metal	L-T	18
D	HAZ	T-L	18
E	Base Metal	T-L	12

Figure 6 - Schematic of Charpy V-Notch Specimen Orientation

28

Figure 7 - S-N Data for Fatigue Cracks in the Electrogas Weld
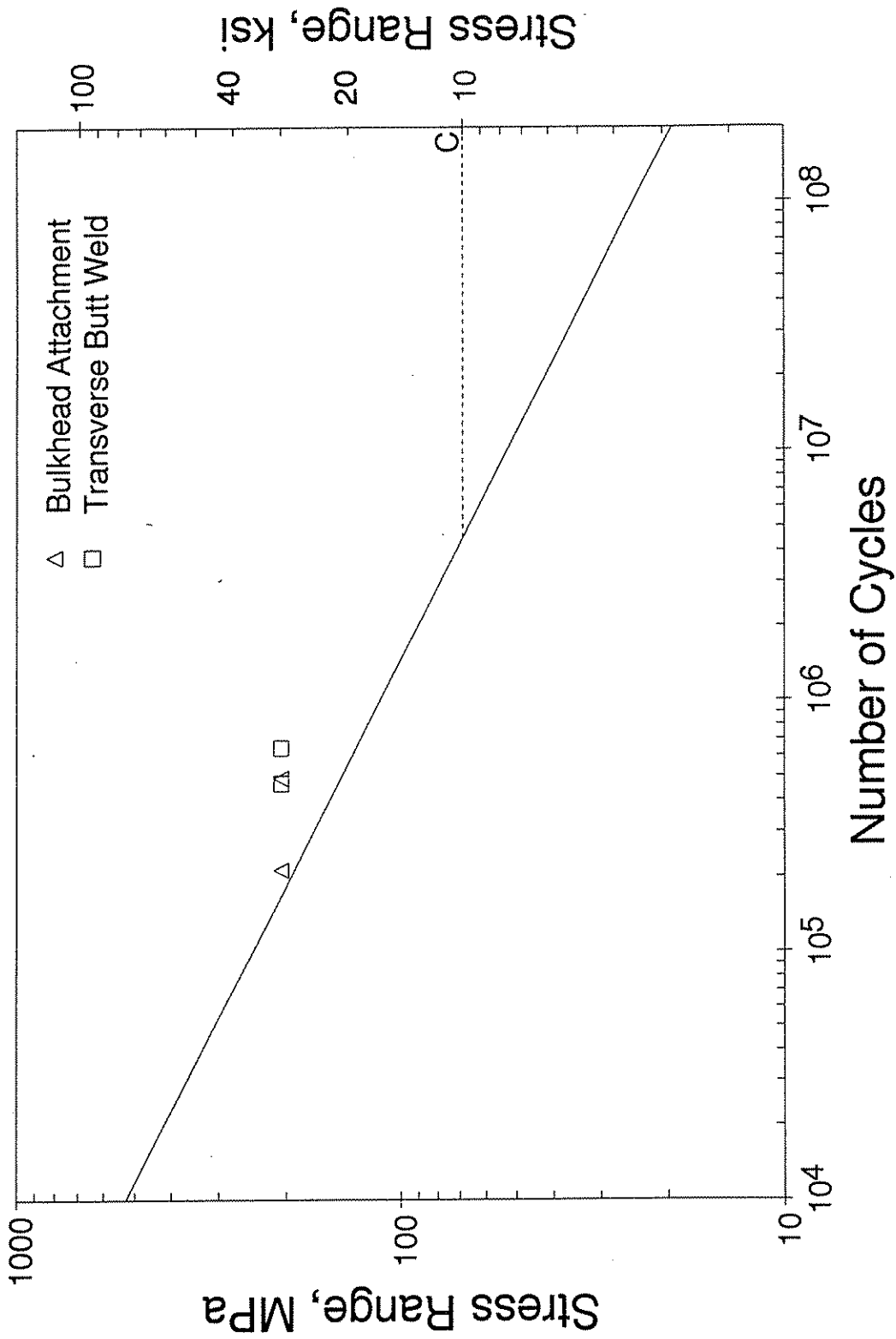
Figure 8 - S-N Data for Fatigue Cracks in Type IIA Specimens

Type II Specimens w/o Bulkhead
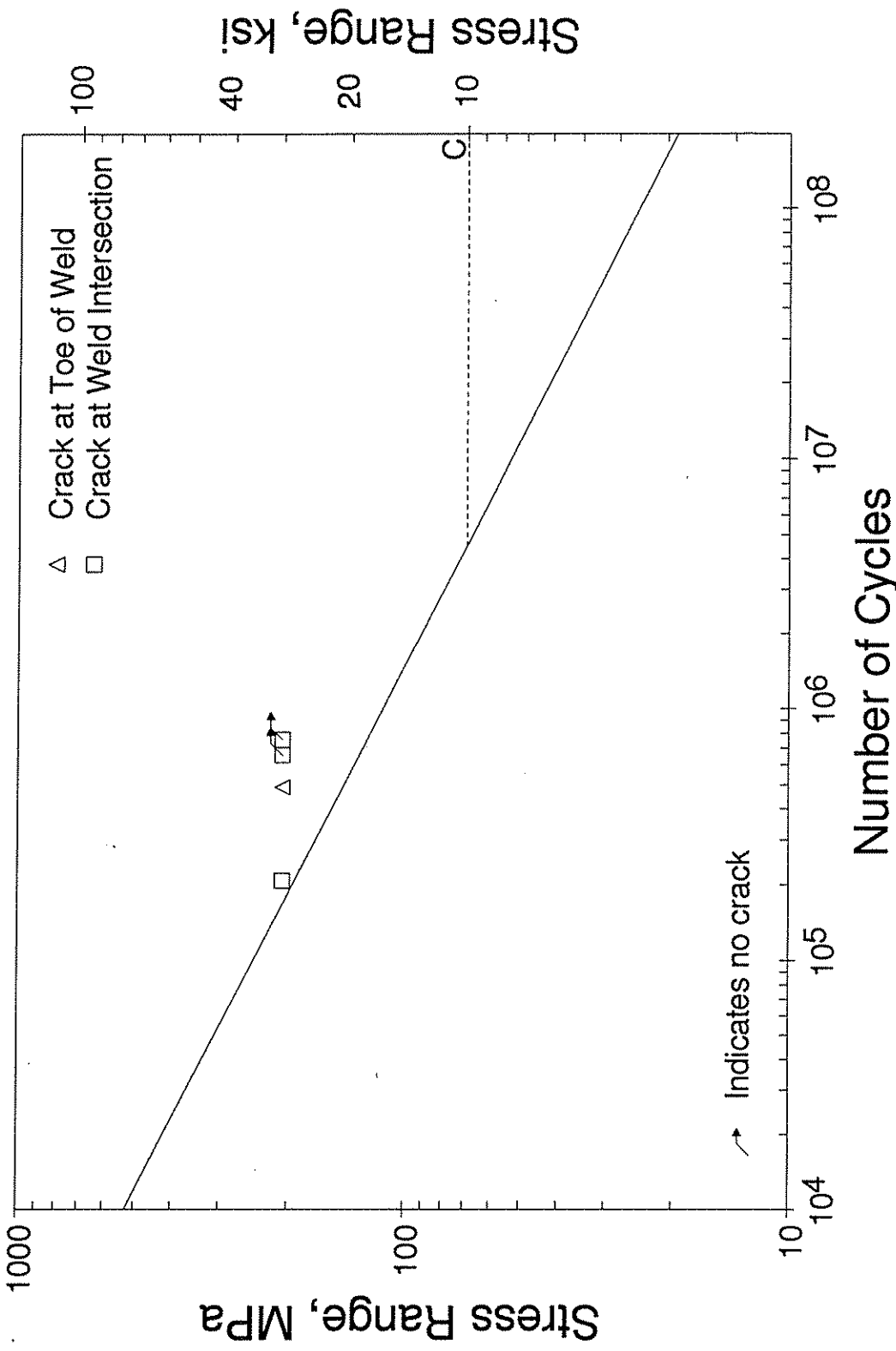
Figure 9 - S-N Data for Fatigue Cracks in Type IIB Specimens

31

Beam: LB 1
Type: II
Stress Range: 207 MPa (30 ksi)
Number of Cycles: 211,900
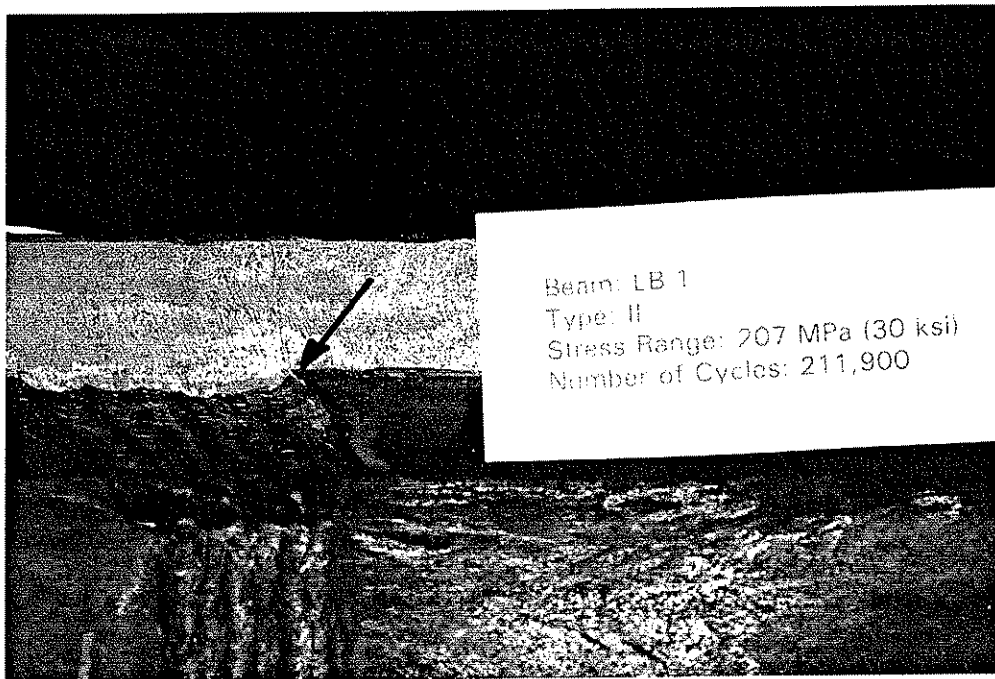
Figure 10 - Fatigue Failure At Toe of Weld on Type IIA Specimen LB-1 (10/93/4-1)
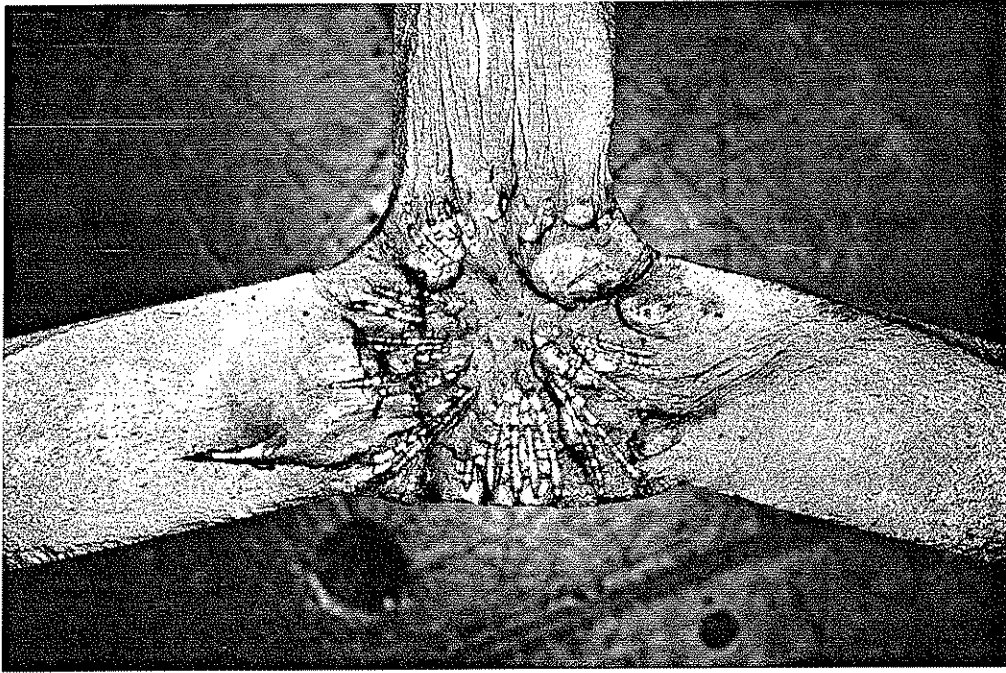
a) Type I Specimen LB-2 (4/93/50-10)

Beam: LB-6(2)
Type: IIB
Stress Range: 207 MPa (30 ksi)
Number of Cycles: 206,000
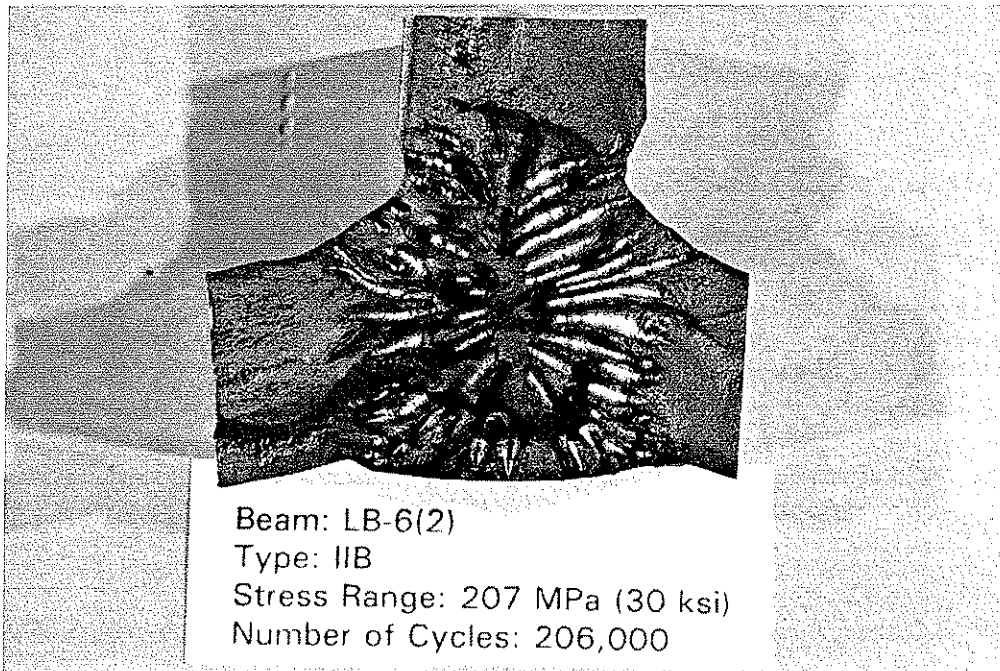
b) Type IIB Specimen LB-6 (12/93/2-10)

Figure 11 - Porosity Defects in Electrogas Weld Material

33
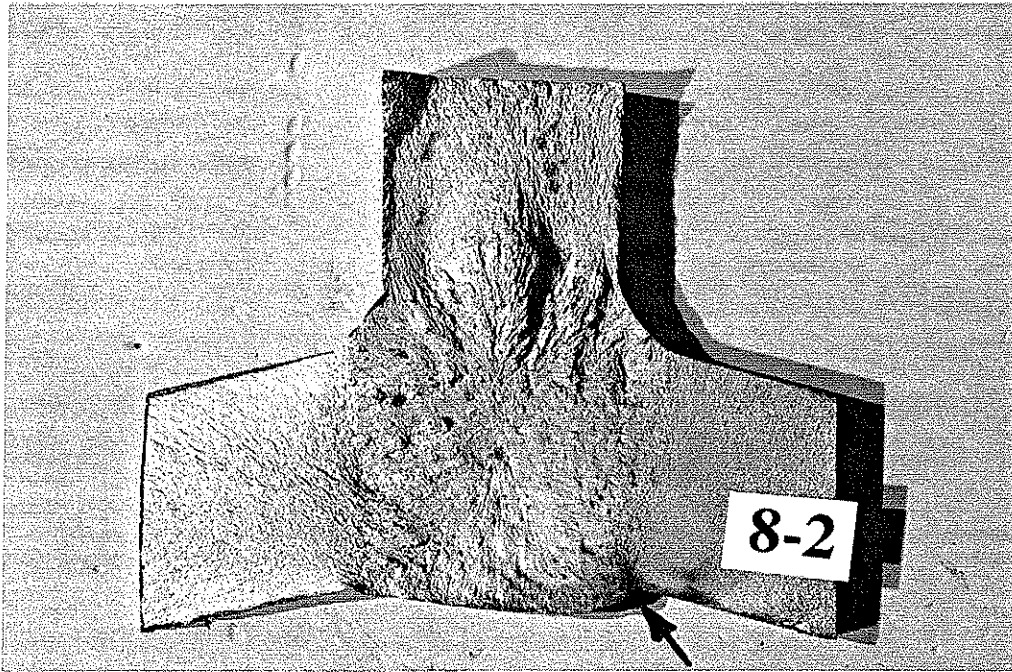
Figure 12 - Fatigue Crack Initiation at the Weld Toe (12/93/24-2)
(Type IIB Specimen LB-8)
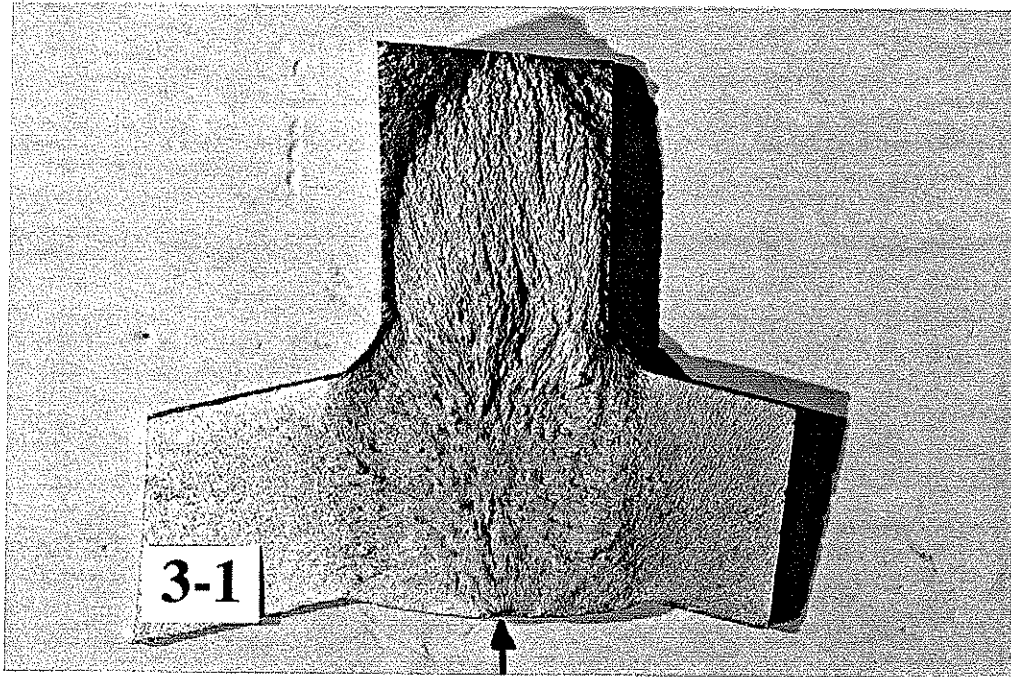
Figure 13 - Fatigue Crack Initiation at a Weld Surface Defect (12/93/24-4)
(Type I Specimen LB-3)

Beam: LB-7(2)
Type: IIB
Stress Range: 179 MPa (26 ksi)
Number of Cycles: 753,800
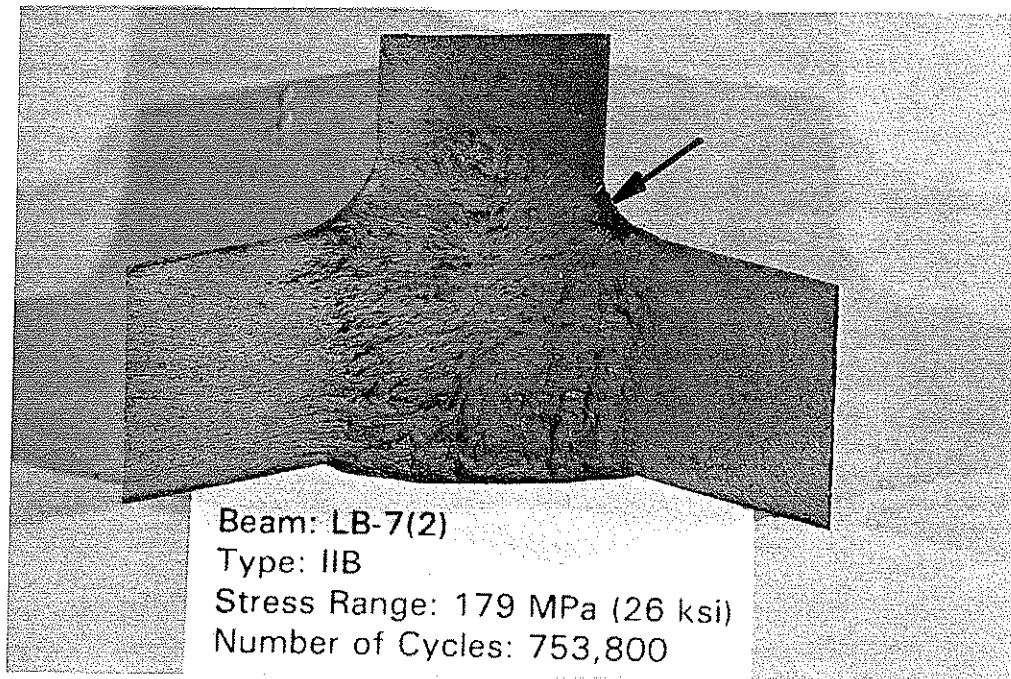
a) Type IIB Specimen LB-7 (12/93/2-12)

Beam: LB-12
Type: I
Stress Range: 242 MPa (35 ksi)
Number of Cycles: 245,000
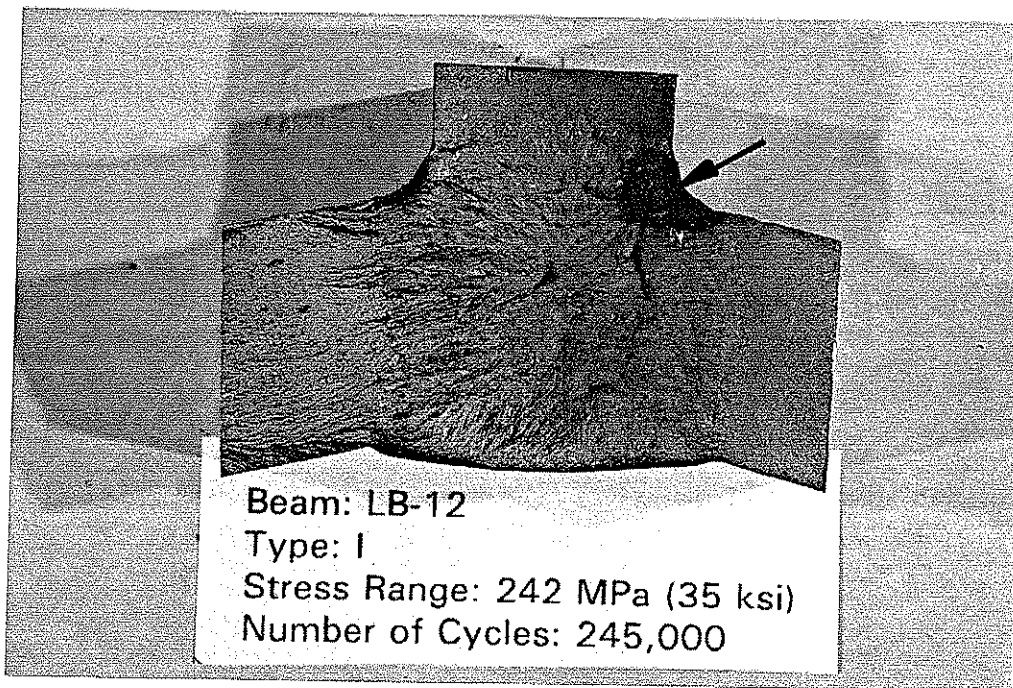
b) Type I Specimen LB-12 (12/93/3-6)

Figure 14 - Fatigue Cracks Initiating at Hydrogen Induced Intergranular Cracks

35
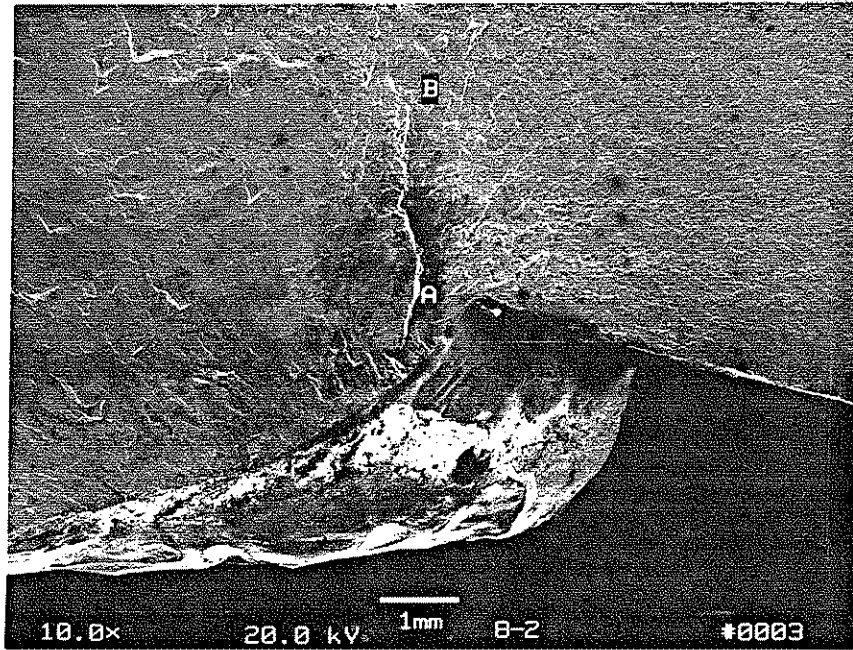
a) Low Magnification View (10x)
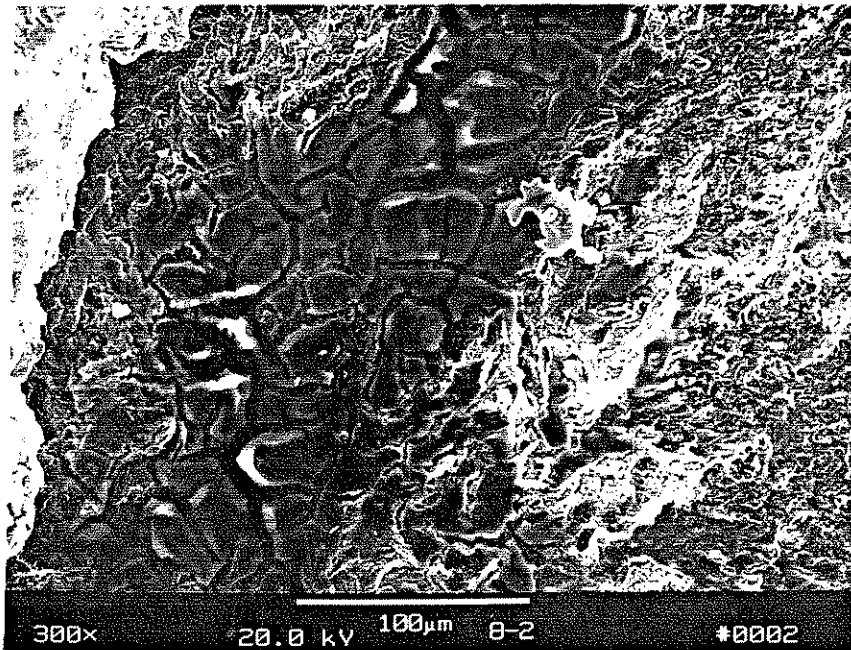
b) Enlarged View of Defect (300x)

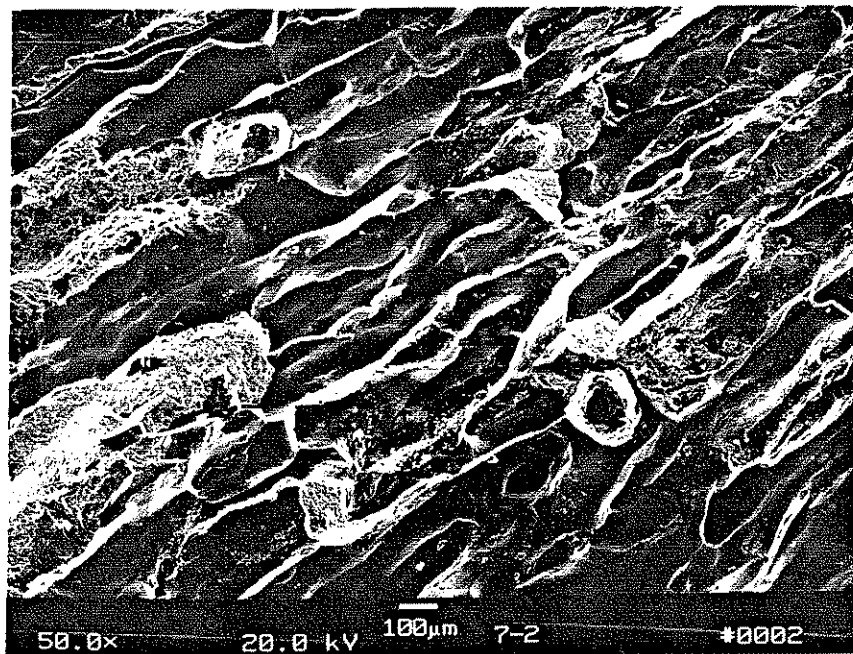Figure 15 - SEM Micrographs of Weld Toe Crack Initiation Site (Type IIB Specimen LB-8)
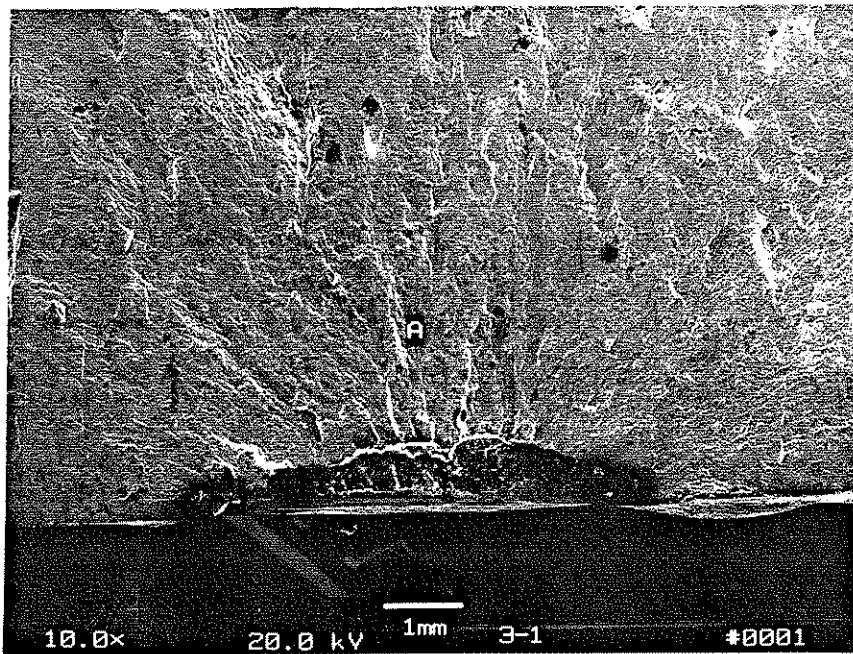
Figure 16 - SEM Micrograph of Fatigue Crack Origin in Type I Specimen LB-3
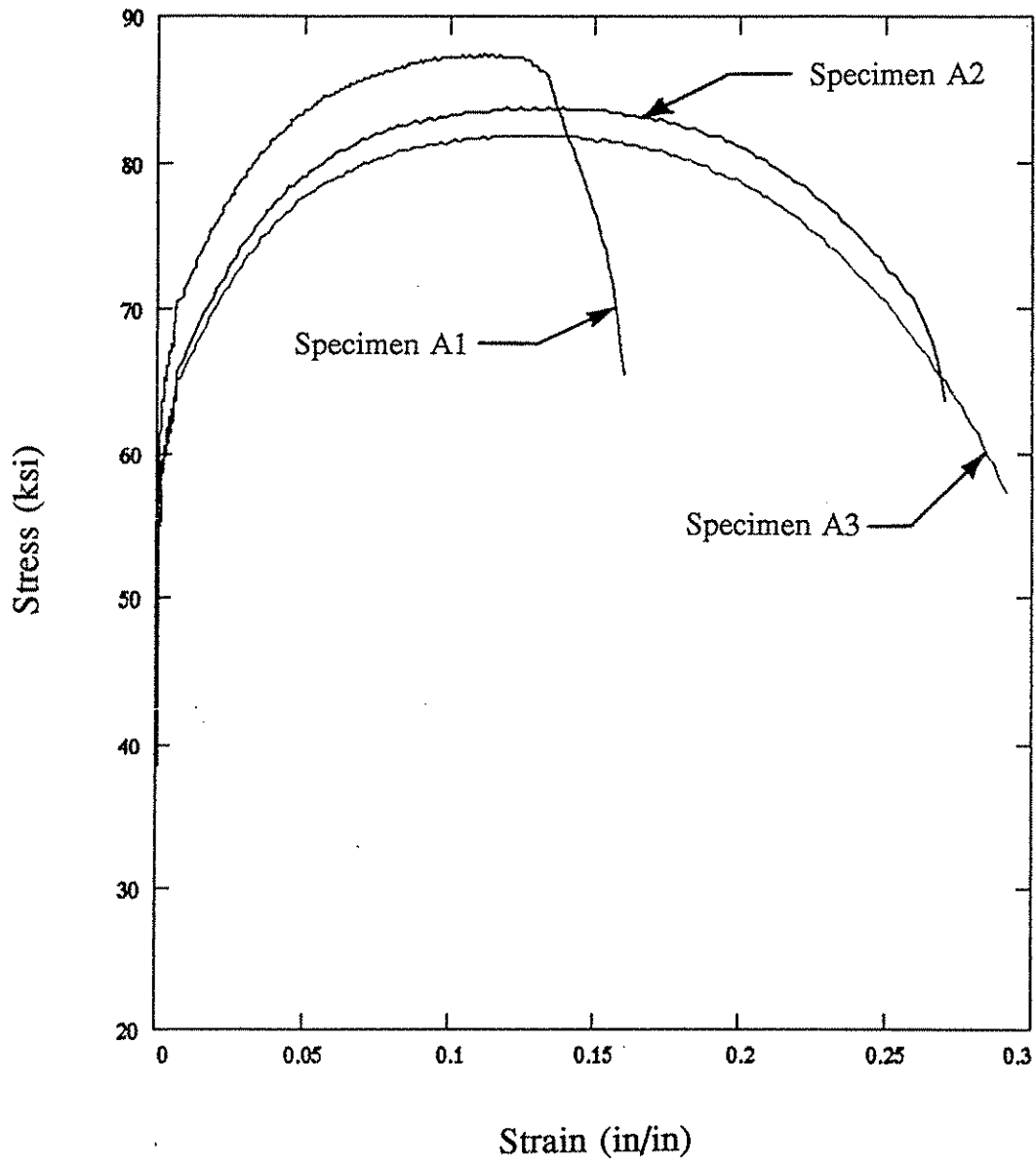(Initiating Defect is a Slag Inclusion at the Weld Surface)
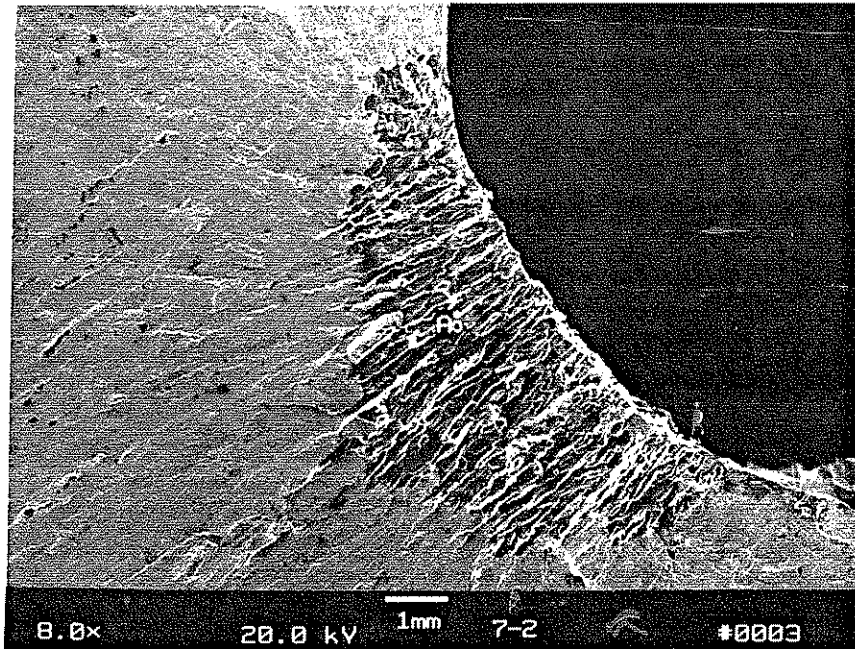
a) Low Magnification View (8x) of Hydrogen Induced Crack

b) Higher Magnification View (50x) of Crack Illustrating Intergranular Fracture

Figure 17 - SEM Micrograph of Fatigue Crack Origin in Type IIB Specimen LB-7

Figure 18 - Stress-Strain Curve for Tension Test of EG82T-G Weld Metal
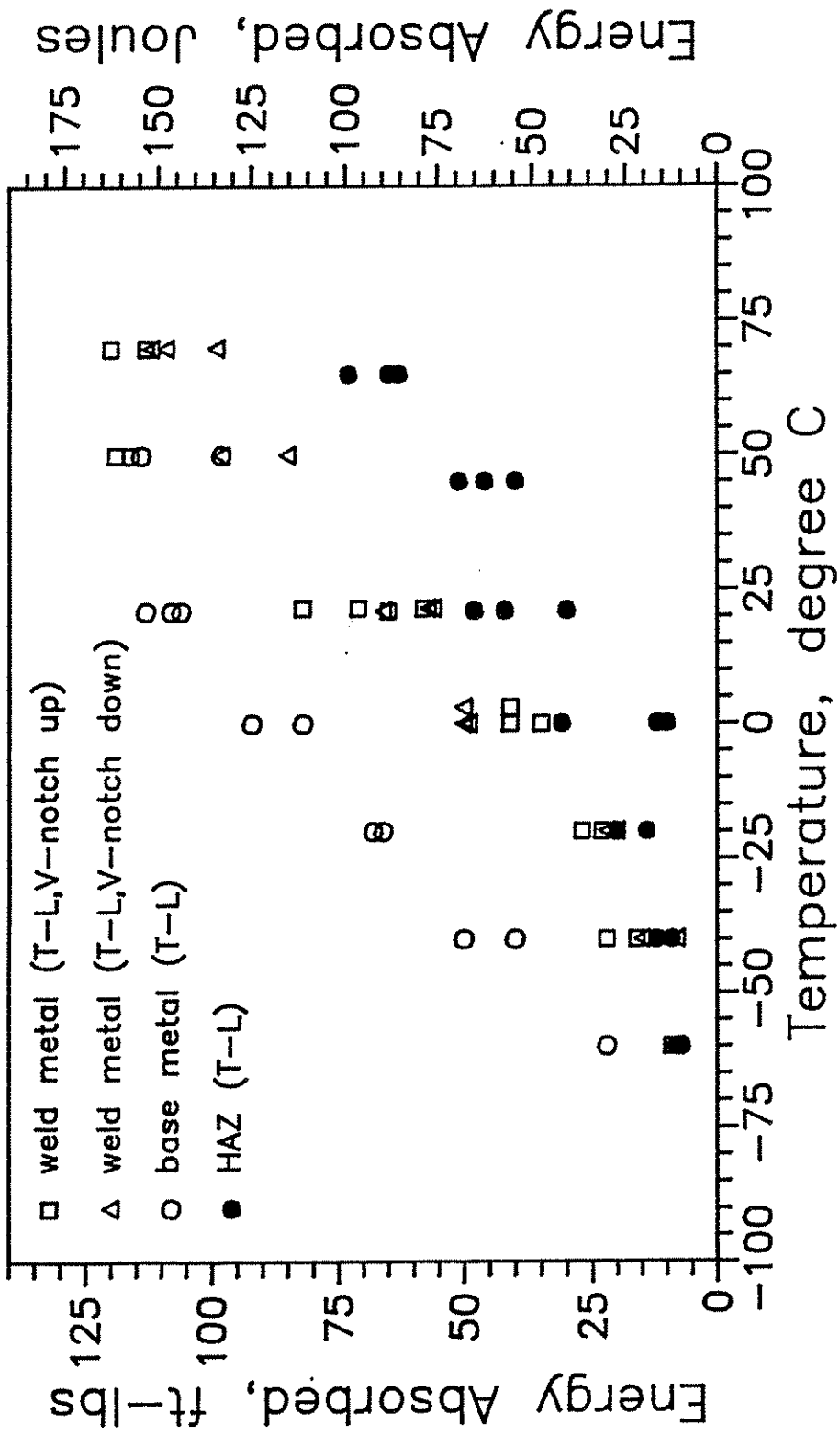
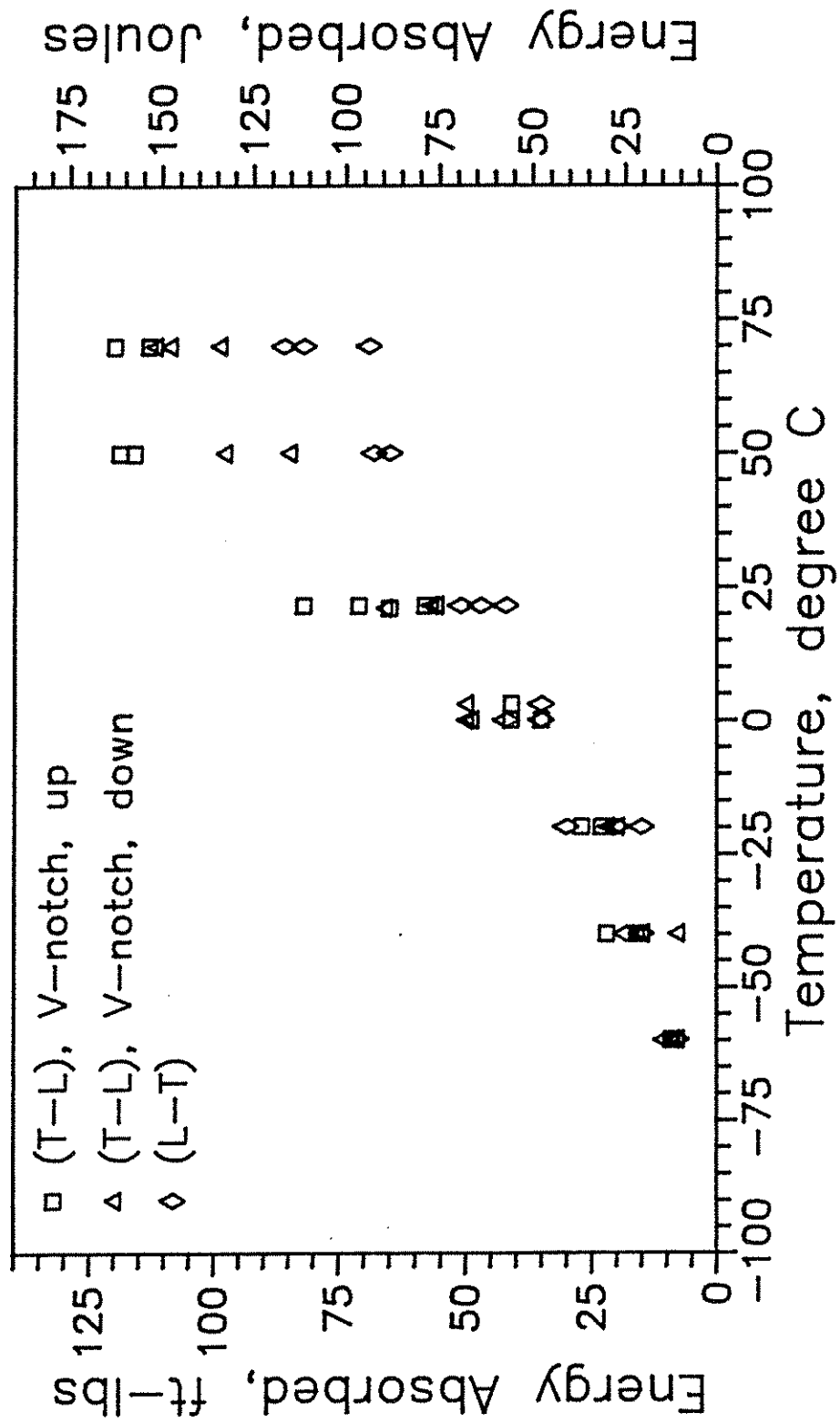Note: 1 ksi = 6.89 MPa

Figure 19 - Charpy V-Notch Test Results

Figure 20 - Weld Metal Charpy V-Notch Test Results

41